Applied Physics A (2020) 126:937
https://doi.org/10.1007/s00339-020-04121-0

Applied Physics A
Materials Science & Processing

Core–shell Ag-ZnO/Curcumin nanocomposite having optically active, thermally stable, hydrophilic surfaces for self cleaning applications

Rajender Singh[1] · Karan Verma[1] · Raj Kumar[1]

Received: 8 May 2020 / Accepted: 31 October 2020

Abstract
In the present manuscript, an effort has been made to develop the curcumin ZnO nanocomposites(CZNCs) for their self-cleaning applications. Presence of ZnO and Ag/ZnO nanoparticles in curcumin matrix get confirmed by X-ray diffraction (XRD) and fourier transform infrared spectrometer (FTIR) techniques. Optimum transparency with tuned refractive index has achieved in Ag/ZnO-curcumin nanocomposite as compared to pure curcumin (Cur). CZNCs show minimum weight loss as compared to Cur sample. Core–shell formation has been further confirmed by selected area electron diffraction (SAED) and high-resolution transmission electron microscopy (HRTEM) studies. The major transition in water contact angle (WCA) to 15.25° for Ag/ZnO-Cur NC (Cur_ZnAg2) from Cur's WCA = 40.55° has been observed. Conclusively, optically active, thermally stable, hydrophilic features based CZNCs can be utilized in self-cleaning applications.

Keywords Nanoparticles (NPs) · Nanocomposites (NCs) · Curcumin (cur) · Transparency · Core–shell

1 Introduction

Turmeric consists of curcumin(Cur), demethoxycurcumin(DMC) and bidemethoxycurcumin (BMC) polyphenolic compounds [1, 2], collectively referred as curcuminoids. Out of them, Cur widely used from "kitchen to clinic" by the people because of its unique properties which have many health benefits [3]. Cur also certified as generally recognised as safe (GRAS) by United state food and drug adminstration (USFDA) [2]. Routinely, Cur (1,7-bis (4-hydroxy-3-methoxyphenyl)-1,6-heptadiene-3,5-dione) [4] used as a food additive for spice and coloring effects (textiles, food & cosmetics) [5]. Upto 10 g/day [6] of Cur can be very well tolerated by humans in nontoxic limits. It is not only used as colouring and spice agent but also used in ayurvedic medical science for more than 4000 years. It is widely accepted and proven fact that Indian old age people between 70 to 79 years who eat curry dishes daily have 4.4 times less vulnerablity towards 'Alzheimer disease' as compared to Americans of same age group [7]. Traditionally, Indians intake Cur in food in various forms strengthen their immune system and develop anticarcinogenic abilities. Moreover, the Cur is also known for its antioxidants [8–10], anti-inflamatory [11] and anticarcinogenic [12] properties, which are quite to treat such stated diseases. Inspite of the therapeutic properties of Cur, its applications are limited due to its poor bioavailability, pharmacokinetics profile & limited solubility in water. To address the stated issues & to enhance the applicability of Cur-based formulations, different systems have been developed with polymer, metals, lipids and inorganic components [13]. Few current studies have been summarized below which were focussed on development of Cur as a hybrid nanocomposite [14–18]. Specifically, to achieve the multifunctional properties of Cur NCs viz. optical, thermal and surface wetting, an attempt has been made to develop Cur based NCs.

In recent time, wide bandgap ZnO nanoparticles (NPs) have drawn more attention as a mixing entity with Cur due to low toxicity on human, plants and animals [19, 20]. These

Electronic supplementary material The online version of this article (https://doi.org/10.1007/s00339-020-04121-0) contains supplementary material, which is available to authorized users.

✉ Rajender Singh
rajenderphysics@gmail.com

Karan Verma
karan.verma49@gmail.com

Raj Kumar
rohit3183@gmail.com

[1] Department of Central Instrumentation Laboratory (CIL), Panjab University, Chandigarh, India

Published online: 16 November 2020

properties can be utilized against different microorganism, anticancer activities and industrial device fabrications [21–23]. Limited research work has been performed on the functionalization of ZnO NPs via organic and inorganic entities [24] for their use in optical, surface wetting & antibacterial applications. Furthermore, Ag has inherent wound healing properties and charge transport abilities due to which it has been used as a dopant in ZnO [25–28]. Originally, ZnO surface equipped with charged trapped states which can be minimized by adsorption or coating of organic compounds on NPs' surfaces [29–32], consequently leads to enhancement of surface plasmon resonance (SPR) [33], photosensetization [34] behaviour.

The limited applications of Cur-based materials in their device fabrications may be due to low thermal stability behavior (maximum decomposition at ~ 400 °C) [17, 35]. In addition to traditional uses, Cur NCs can be developed as multifunctional material by incorporation of ZnO & Ag/ZnO NPs in Cur matrix. Apart from this, the use of Cur with ZnO NPs brings the composite to least toxicity level and restricts the generation/growth of hydroxyl radical, singlet oxygen, lipid peroxidation etc. entities [36, 37]. Due to the above-stated features of Cur NCs, it can be used in different food packaging applications [38].

Coating surfaces become very popular & get utilized in different applications to protect the materials' surface texture, window glasses and different open-air devices from external natural or man-made deteriorating factors such as dirt, dyes & other contaminants. Deposited impurities can be removed with hydrophilic or hydrophobic behavior [39] irrespective to the structural & chemical properties of the studied material. Hydrophilic behavior can be achieved through the presence of hydroxyl, carboxyl, sulphonic group etc., whereas the presence of nonpolar groups on sample surfaces bring hydrophobic nature [39], towards self-cleaning behavior of synthesized material surfaces.

In literature, different nanocomposites (NCs) have been studied with semiconductor as one of the component [39–45] with reference to surface wetting behavior. In addition to the properties of base material i.e. Cur (environmental friendly [3–6]), features and concentration of nanofillers have equally dominated the desired hydrophilic behavior. Current reported results w.r.t. hydrophilic nature of CZNCs, are found in the same trend as already reported by researchers [40, 41, 45].

In the current manuscript, the idea to work with curcumin ZnO nanocomposites (NCs) was based to develop CZNCs having hybrid properties with enhancement in its thermal stability [17, 35], so that we can use reported NCs in surface cleaning applications. Furthermore, desired hydrophilic properties of NCs can be achieved with optimum refractive index(n), roughness and uniform dispersion of ZnO NPs in Cur matrix. Moreover, the above-desired properties can be achieved by appropriate synthesis method, proper homogenization of mixing entities together. Overall, the effect of ZnO, Ag/ZnO with variable content of Cur and Ag/ZnO for different CZNCs have been studied in the current manuscript for self cleaning applications.

2 Experimental section

2.1 Material and methods

Purified form of curcumin (batch no. NCE/292,014) has been received from Sunpure Extracts Pvt. Ltd, New Delhi. Zinc nitrate hexahydrate (99.0%), Silver nitrate ($AgNO_3$) and sodium hydroxide (98.56%) have been used in the synthesis of ZnO, Ag and Ag/ZnO NPs. Neem extract of fresh leaves from Panjab University Chandigarh campus (India) has been used as a reducing agent for the preparation of NPs. Triple distilled water has been used in the different synthesis process.

2.2 Synthesis

2.2.1 Preparation of neem extract

Neem fresh leaves (10 g) extract has been prepared through proper washing of neem leaves with distilled water and drying them in shades. Furthermore, the dried leaves were grinded to coarse powder followed by extraction with 100 ml triple distilled water prior to their evaporation to get crude extract at 80 °C (Step 1).

2.2.2 Preparation of silver (Ag) nanoparticles (NPs)

0.005 M of $AgNO_3$ has been dissolved in triple distilled water (50 ml) at appropriate stirring speed. 2 ml volume of neem extract synthesized in step 1, has been added dropwise to $AgNO_3$ solution. Complete reaction set up shifted to a water bath at 80 °C temperature for 2 h. Finally, the solution's colour changes to dark brown from pale yellow which confirmed silver precursor reduction into Ag NPs (Step 2).

2.2.3 Preparation of Ag-doped ZnO(Ag/ZnO) NPs

0.02 M amount of $Zn(NO_3)•6H_2O$ has been dissolved in triple distilled water (50 ml) at appropriate stirring speed. 30 ml of Ag NPs solution (prepared at step 2) added dropwise with proper stirring. Moreover, 10 ml of neem extract (prepared at step 1) has been also added dropwise to the last solution. To ensure complete precipitation of zinc precursor, 50 ml of 1 M NaOH solution added dropwise to the above solution. Whole reaction set up has been shifted to a water bath at 80 °C temperature for 2 h. Finally, the solution's

colour changes to deep yellow paste, which indicates the formation of ZnO NPs (Step 3). Similar steps have been followed for pure ZnO NPs synthesis with absence of Ag NPs (Step 4). Pure ZnO and Ag-doped ZnO (Ag/ZnO) NPs have been annealed at 400 °C for 2 h. The pH of NCs samples including pure curcumin dissolved in dimethylsulfoxide (DMSO) was observed of value i.e. 9.50 (basic nature).

2.2.4 Preparation of Cur(Zn)O & Cur(Ag/Zn)O nanocomposite

CZNCs have been synthesized by mixing of Cur, ZnO and Ag/ZnO NPs in different proportions. Already dissolved 250 mg of curcumin in 50 ml distilled water follows with the addition of the same amount of ZnO NPs (synthesized in step 4) through vigorous stirring for 4 h at 60 °C. Final solution was dried at ~ 45 °C for 24 h, followed with vacuum drying for 24 h. In the next samples, ZnO NPs have been replaced with Ag/ZnO NPs (Step 3) into Cur.

To study the effect of Cur and Ag/ZnO in their NCs, the contents of Cur and Ag/ZnO NPs have been incorporated in vice versa manner. The pure Cur, ZnO & Ag/ZnO based Cur NCs were named as Cur, Cur_Zn & Cur_ZnAg respectively. Two more samples have been synthesized with variation in the ratio of Cur & Ag/ZnO NPs, which were coded as Cur_ZnAg1 (curcumin is 333 mg + 167 mg of Ag/ZnO), Cur_ZnAg2 (curcumin is 167 mg + 333 mg of Ag/ZnO) respectively. To study the different properties of CZNCs, samples were deposited on ~ $2 \times 2 cm^2$ glass substrate by dip-coating method. Figure 1 proposed the reaction mechanism depicting the formation of CZNCs with probable interaction sites between reacting species.

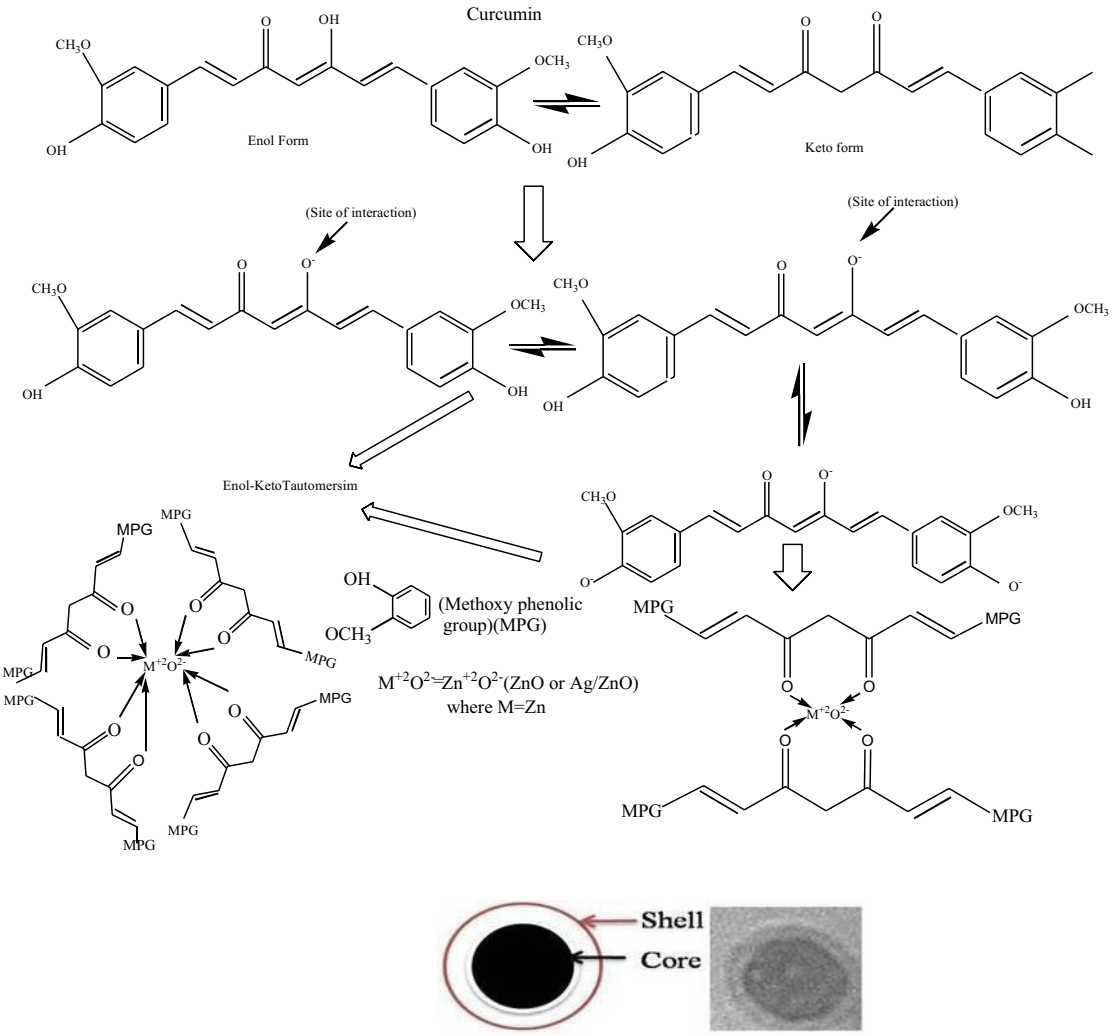

Fig. 1 Proposed reaction mechanism of CZNCs

2.2.5 Characterization techniques

The crystal structure of CZNCs was studied with the help of X-pert pro diffractometer (Panalytical) at λ = 1.54 Å. Fourier transform infrared spectrophotometer (FTIR) has been employed to investigate the chemical structure of synthesized samples in mid-infrared range (400–4000 cm^{-1}). Ultra-Violet–Visible spectrophotometer (UV–Vis) (Perkin Elmer lamda 750) technique has been used to explore the transmittance, refractive index behavior of prepared thin films from wavelength 200 to 800 nm. Thermogravimetric analysis (TGA) study has been performed to analyze the thermal behavior of synthesized NCs. Field emission scanning electron microscopy (FESEM) (Hitachi SU8010) with energy dispersive spectroscopy (EDS) X-flash Japan has been used to study the surface morphology and elemental distribution of CZNCs thin films. Transmission electron microscopy (TEM) Hitachi's H7500 and High-Resolution TEM (HRTEM) Joel 2100 Plus have been used to explore ultra-structural information of synthesized NCs. Surface roughness of different synthesized thin films has been analyzed using NT-MDT atomic force microscope (AFM). The water contact angle (WCA) measurements of different CZNCs with water droplet of 10 µl were studied using DSA100 (Kruss make) system.

2.2.6 X-ray diffraction (XRD) measurement

The ZnO and Ag/ZnO NPs have been synthesized by green synthesis approach. In figure supplimentary(S) file S1(a), shows ZnO NPs diffraction peaks at 31.73(100), 34.44(002), 36.31(101), 47.51(102), 56.50(110), 62.94(103), 66.50(112), 68.02(201) & 69.22(202) respectively. Presence of these peaks confirms the hexagonal wurtzite structure of ZnO [46, 47]. No diffraction peaks of silver metal have been observed in ZnO diffraction pattern in Ag/ZnO sample. Absense of Ag peak in Ag/ZnO diffraction pattern confirms the complete replacement of Ag^{+} (ionic radii = 0.126 nm) with Zn^{+2} (ionic radii = 0.074 nm) ions in ZnO matrix. Incorporation of Ag into ZnO matrix brings a slight increase in the diffraction intensity for (101) peak [48]. Incorporation of silver metal into ZnO crystal structure brings a decrease in crystallite size (for 101 peak) to 24.93 nm from 30.09 nm (ZnO) respectively. Furthermore, the effect of ZnO, Ag/ZnO & curcumin concentration on the crystal structure of CZNCs also has been investigated in Fig. 2.

In Fig. 2(i), diffractogram (a) confirms the amorphous nature of curcumin as no sharp peak has been observed. Furthermore, the Cur_Zn sample (Fig. 2-ib) shows the presence of ZnO diffraction peaks prominently for (100), (002) & (101) (hkl) planes. In Cur_Zn NC, the ratio of curcumin and ZnO was 1:1, which may be the probable reason of low-intensity diffraction peaks of ZnO reflections. In Cur_ZnAg sample, ZnO has been replaced with Ag/ZnO. Small crystallite size of Ag/ZnO NPs i.e. 24.93 nm as compared to ZnO size 30.09 nm, may be the possible reason to bring agglomeration of Ag/ZnO NPs in Cur matrix which shows the low intensity of (101) reflection peaks in Cur_ZnAg2 as compared to Cur_ZnAg1 (Fig. 2i-b).

2.3 FTIR study

FTIR spectroscopy has been used to study ZnO, Ag/ZnO NPs' interaction with Cur which is shown in Fig. 3i–v. Figure 3(i) shows the detailed spectrums from 400 to 4000 cm^{-1} for pure ZnO(a), Ag/ZnO(b), Cur(c), Cur_Zn(d), Cur_ZnAg(e), Cur_ZnAg1(f) & Cur_ZnAg2(g) samples respectively. Zn–O absorption band of pure ZnO & Ag/ZnO found to be shifted to lower frequency from 476 cm^{-1} (ZnO & Ag/ZnO) [49] to 447 cm^{-1} (Cur_Zn), 465 cm^{-1}(Cur_ZnAg), 459 cm^{-1} (Cur_ZnAg1) & 458 cm^{-1} (Cur_ZnAg2) respectively. The shifting of Zn–O vibration to lower wavenumber

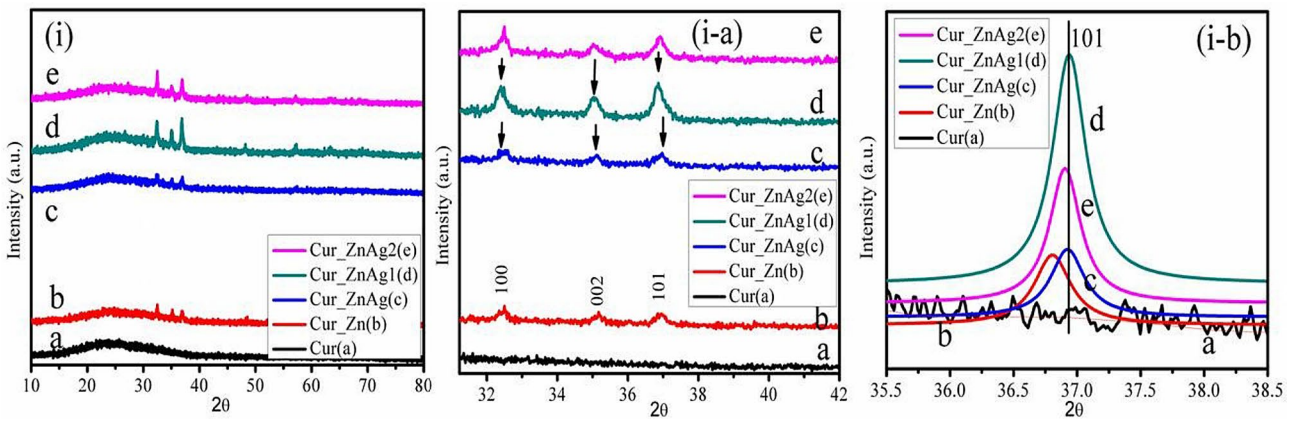

Fig. 2 **i** Shows the diffraction pattern of Cur, Cu_Zn, Cur_ZnAg, Cur_ZnAg1, Cur_ZnAg2, **i-a** diffraction pattern from 2θ = 31° to 42°, **i-b** Gaussian fit of corresponding (101) peak respectively

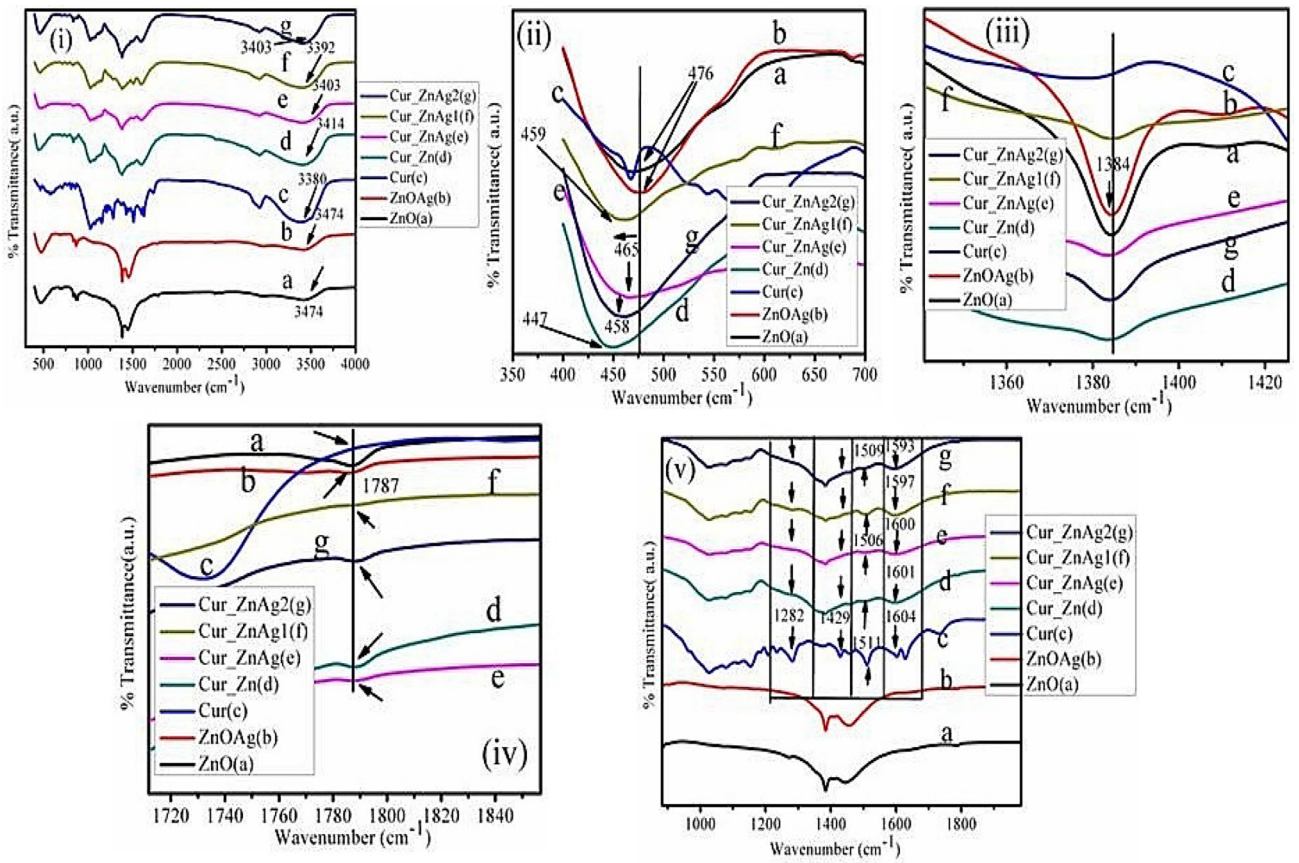

Fig. 3 FTIR spectra of **i** different synthesized NCs, **ii** frequency range from 350 to 700 cm^{-1} **iii** from 1360 to 1420 cm^{-1}, **iv** from 1720 to 1840 cm^{-1} **v** from 1000 to 1800 cm^{-1} respectively

in CZNCs confirms the effective chemical interaction between Cur and ZnO, Ag/ZnO respectively. In Fig. 3(iii & iv), band vibrations at 1384 cm^{-1}, 1787 cm^{-1} represent the presence of C = O stretching vibration of carboxylic group [50]. The presence of the above two bands shows the abundance of phenolic acid, terpenoids and protein on ZnO and Ag/ZnO surface, which surely released from A. indica leaf extract. Furthermore, after the interaction of NPs with Cur, the intensity and width of the corresponding peaks have been drastically changed (Fig. 3iii, iv).

In addition, the FTIR spectrum of Cur has been investigated in detail by Fig. 3i, v. Figure 3i spectrum (c-g), the phenolic –OH peak stretching shifted to higher frequency from 3380 cm^{-1} to 3414 cm^{-1}, 3403 cm^{-1}, 3392 cm^{-1}, 3403 cm^{-1} for Cur, Cur_Zn, Cur_ZnAg, Cur_ZnAg1, Cur_ZnAg2 respectively. Apart from shifting of phenolic –OH band vibration, a prominent change has been observed in the intensities of corresponding bands' vibration, which predicts the alteration in the chemical structure of Cur. The presence of phenolic –OH group in Cur structure induces hydrophobic character of the composite and further modification in CZNCs structure brings effectiveness in properties like thermal stability, solubility etc. [51].

In Fig. 3v, the frequency region from 1000 to 1800 cm^{-1} depicts, the frequency band vibration for aromatic C–O stretching (1282 cm^{-1}), olefinic C–H bending vibration (1429 cm^{-1}), C–O, C–C band vibration (1511 cm^{-1}) and benzene vibration band (1604 cm^{-1}) [52]. With incorporation of ZnO and Ag/ZnO NPs into Cur, the above frequency vibration for aromatic C–O stretching vibration & olefinic C–H vibration get diminished to minimum level. Furthermore, the 1511 cm^{-1} (Cur) band vibration shifted to 1506 cm^{-1} (Cur_ZnAg), 1506 cm^{-1} (Cu_ZnAg1) & 1509 cm^{-1} (Cur_ZnAg2), respectively. Similarily, the benzene vibration band position also shifted to lower frequency band i.e. from 1604 cm^{-1} (Cur) to 1601 cm^{-1} (Cur_Zn), 1600 cm^{-1} (Cu_ZnAg), 1597 cm^{-1} (Cur_ZnAg1) & 1593 cm^{-1} (Cur_ZnAg4) respectively as shown in Fig. 3v. Overall, the shifting and modification in Cur and NPs vibration bands after mixing with ZnO & Ag/ZnO NPs (Fig. 3ii–v) confirms their chemical interaction in respective NCs.

2.4 UV–Vis spectroscopy

The synthesized NCs thin films have been studied for their transmittance, refractive index (n) & optical band gap (E_g) behavior as shown in Figs. 4 and S2. Figures 4i, ii, show the transmittance and refractive index of synthesized thin films. The % transmittance values change from 71.32 for Cur to 19.17, 17.54, 39.06, 24.06 for Cur_Zn, Cur_ZnAg, Cur_ZnAg1, Cur_ZnAg2 respectively. Similarily the refractive values(n) and optical band gap(E_{opt}) values for corresponding samples have been tuned from 2.01 to 2.40, 3.08, 1.98, 2.70 and 2.38 eV to 2.80 eV, 2.72 eV, 2.88 eV, 3.04 eV respectively.

The incorporation of ZnO NPs into Cur i.e.(Cur_Zn sample, curve 4-ib) brings a decrease in the transmittance from 71.32% (Cur) to 19.17% (Cur_Zn) at 550 nm(Fig. 4ii). The drastic change has been observed in Cur_Zn thin-film transmittance behavior as compared to Cur sample, which is probably due to the effective chemical interaction between Cur and ZnO NPs [53]. In Cur_ZnAg sample, the presence of Ag/ZnO NPs in Cur has brought down the transmittance to 17.54%. Furthermore in Cur_ZnAg1, the content of Cur is double as compared to Ag/ZnO NPs which increased the transmittance to 39.06%. Moreover in Cur_ZnAg2 sample, the content of Ag/ZnO is reversed with Cur as compared to Cur_ZnAg1, which decreased the transmittance to 24.06%. This probably may be due to the presence of more absorption sites(Ag/ZnO) in Cur matrix.

The transmittance (T) for synthesized thin films was calculated from Eq. 1 [54]:

$$T = Aexp(-\alpha d) \tag{1}$$

where T, d are the transmittance, thickness and A is constant.

Refractive index of synthesized thin films has been evaluated with the help of Eq. (2) [55]:

$$n = \frac{1+R}{1-R} + [\frac{4R}{(1-R)^2} - k^2]^{1/2} \tag{2}$$

where R, k are reflectance, extinction coefficient, respectively.

The optical band gap (E_g) of synthesized thin films was calculated from Eq. (3) [56]:

$$\alpha h\nu = D(h\nu - E_g)^n \tag{3}$$

where $h\nu$, E_g, D are photon energy, optical band gap and constant respectively. For ZnO nanomaterial (direct band gap) n = 1/2 gives the best linear curve in band edge region [51].

A detail tauc plot for different studied thin films has been summarized in figure S2.

Incorporation of ZnO NPs into Cur matrix leads to reorganization of valance band (VB) and conduction band (CB) of studied samples, which brings modification in corresponding band gaps (E_g). The blue shift in band gap has been observed from Cur to Cur_ZnAg2 (2.38 eV to 3.04 eV) except Cur_ZnAg (2.72 eV). This may be due to small crystallite size of Ag/ZnO NPs in comparison to ZnO NPs as observed in XRD study (Fig. 2) [57]. Figure 5 have diagramatically illustrated the physical appearance of synthesized thin films w.r.t. transparency behavior. Furthermore, figure S3 depicted the cross-sectional view of synthesized thin films by FESEM technique. Deposited thickness of Cur, Cur_Zn, Cur_ZnAg, Cur_ZnAg1, Cur_ZnAg2 thin films have value viz. 640 nm, 1065 nm, 1060 nm, 1114 nm, 1192 nm, respectively.

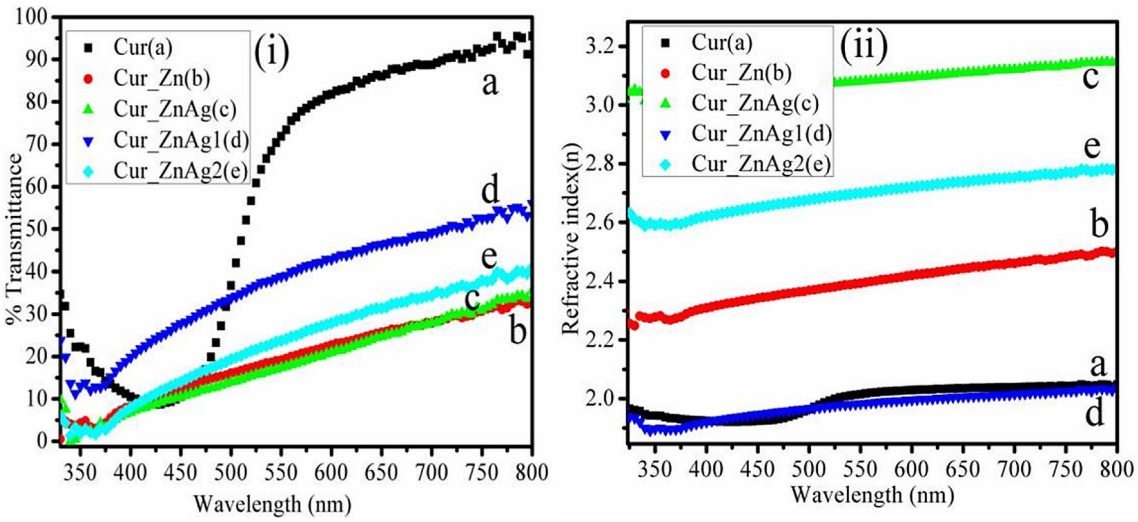

Fig. 4 UV–Visible study shows **i** % transmittance of different thin film samples, **ii** their refractive index (n) behavior respectively

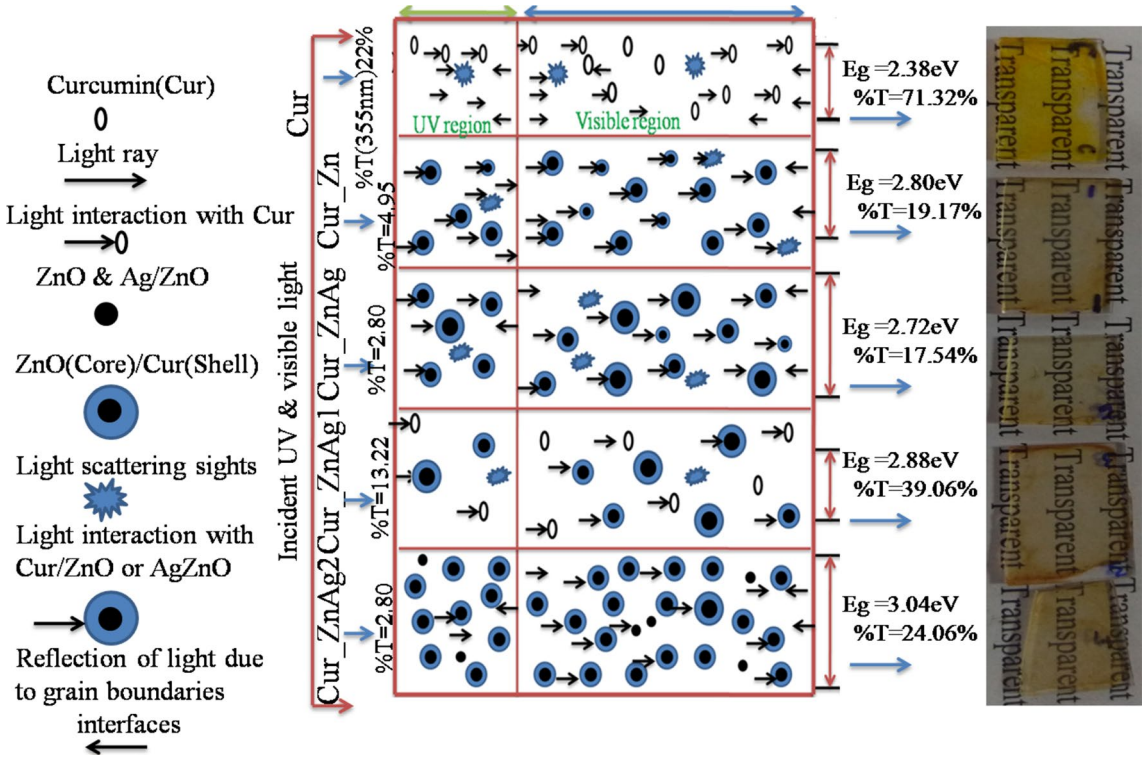

Fig. 5 Schematic representation of light interaction with CZNCs

2.5 Thermal studies

TGA analysis for Cur, Cur/ZnO & Cur-Ag/ZnO NCs has been studied in Fig. 6(i, ii and iii). Figure 6i depicted the thermal degradation behavior of Cur, Cur_Zn, Cur_ZnAg, Cur_ZnAg1 & Cur_ZnAg2 NCs from 30 to 950 °C. Initially degradation at 200 °C, weight loss viz. 6%, 15%, 16%, 15% & 10% has been observed for Cur, Cur_Zn, Cur_ZnAg, Cur_ZnAg1 & Cur_ZnAg2 respectively as shown in Fig. 6ii. Initial loss in weight for Cur sample may be due to Cur's dihydroxylation -OH group which additionally get enhanced in NC samples. This may be due to increased -OH group from ZnO surface [58]. Also the hydrophobic nature of Cur [59] may be one more reason

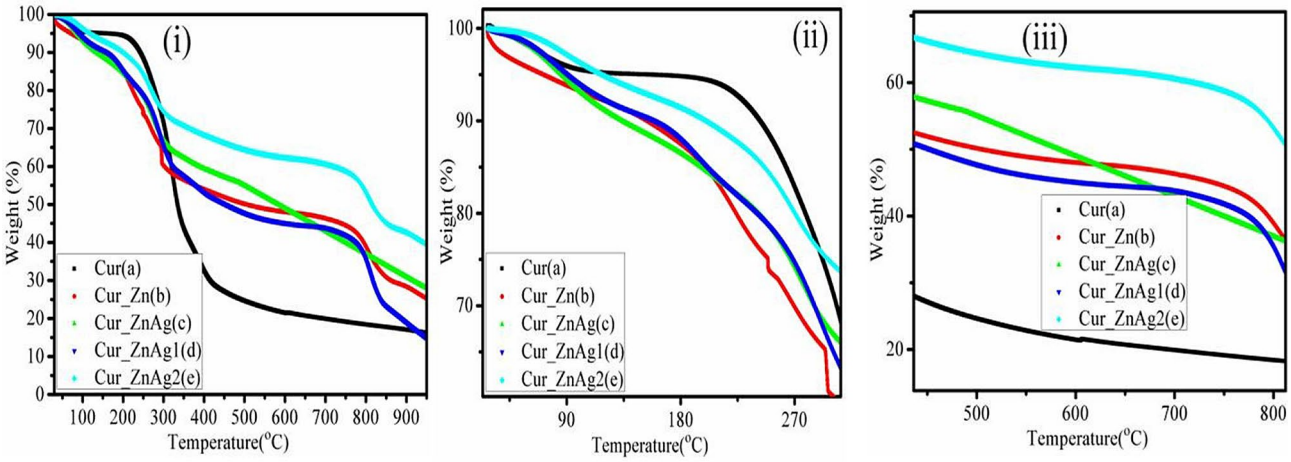

Fig. 6 TGA behavior of **i** Cur(a), Cur_Zn(b), Cur_ ZnAg(c), Cur_ZnAg1 (d),Cur_ZnAg2(e) **ii** zoomed x-axis in temperature range from 30 to 280 °C for initial thermal degradation, **iii** zoomed x-axis in temperature range from 450 to 800 °C for thermal degradation respectively

for delayed –OH group related weight loss of Cur sample as compared to CZNCs [60].

Furthermore, at 400 °C, a sharp weight loss of Cur sample has stimulated the slow degradation behavior of different CZNCs. This may be due to interaction between Cur, ZnO and Ag/ZnO NPs as previously confirmed by FTIR study in Fig. 3. In Fig. 6iii, at 800 °C temperature, 82%, 60%, 43%, 65% & 47% weight loss has been observed for Cur, Cur_Zn, Cur_ZnAg, Cur_ZnAg1 & Cur_ZnAg2 respectively. The second highest weight loss (65%) in Cur_ZnAg1 sample has been observed after Cur sample, which may be due to the presence of high content of Cur. The presence of crystalline ZnO & Ag/ZnO NPs in Cur matrix may be the possible reason for delayed thermal degradation of studied NCs [35].

2.6 FESEM study

Morphological investigation of synthesized ZnO, Ag & Ag/ZnO NPs has been demonstrated in Fig. 7a–c by FESEM technique. Nearly spherical particles of ZnO have been observed in Fig. 7a. The incorporation of spherical shape Ag NPs (Fig. 7b) into zinc precursor has brought no major modification in the morphology of ZnO (Fig. 7c).

The ultrastructural morphology of synthesized ZnO, Ag & Ag/ZnO NPs has been analysed by TEM study as shown in Fig. 8a–c. Average particle size value viz. 34.65 nm, 21.77 nm & 28.65 nm have been observed for pure ZnO, silver(Ag) & Ag/ZnO NPs respectively. Above observed trend of decrease in particle size with the addition of Ag into ZnO matches with crystallite size values of XRD study (Figure S1).

The morphological investigation, elemental presence with distribution behavior of different CZNCs have been summarized in Figs. 9a–e, Fig. 10a–e & Fig. 11a–e respectively. No specific morphology of Cur thin film has been observed in Fig. 9a. Nearly spherical shape transformation in Cur_Zn NC takes place (Fig. 9b) with the incorporation of ZnO NPs in Cur matrix. Similar behavior has been observed in Cur_ZnAg with the incorporation of Ag/ZnO NPs in Cur (Fig. 9c). Cur_ZnAg1 NC shows uniform distribution of spherical entities which may be due to homogenous dispersion of Ag/ZnO NPs in Cur matrix.

In continuation, Cur_ZnAg2 sample in Fig. 9e shows non uniformity of NPs in its NC, may be due to aggregation of Ag/ZnO NPs. Same hypothesis has been confirmed in XRD study as Cur_ZnAg1 shows higher crystallinity behavior (Fig. 2), lowest refractive index (1.98) and optimum transparency (39.08%) in Fig. 4i, ii. Homogenous dispersion of mixing species (Cur & NPs) together may be the reason behind higher crystalline, optimum refractive index and transparency nature of Cur_ZnAg1 NC.

Detail values of wt% of different elements in studied NCs have been summarized in Fig. 10a–e and Table 1.

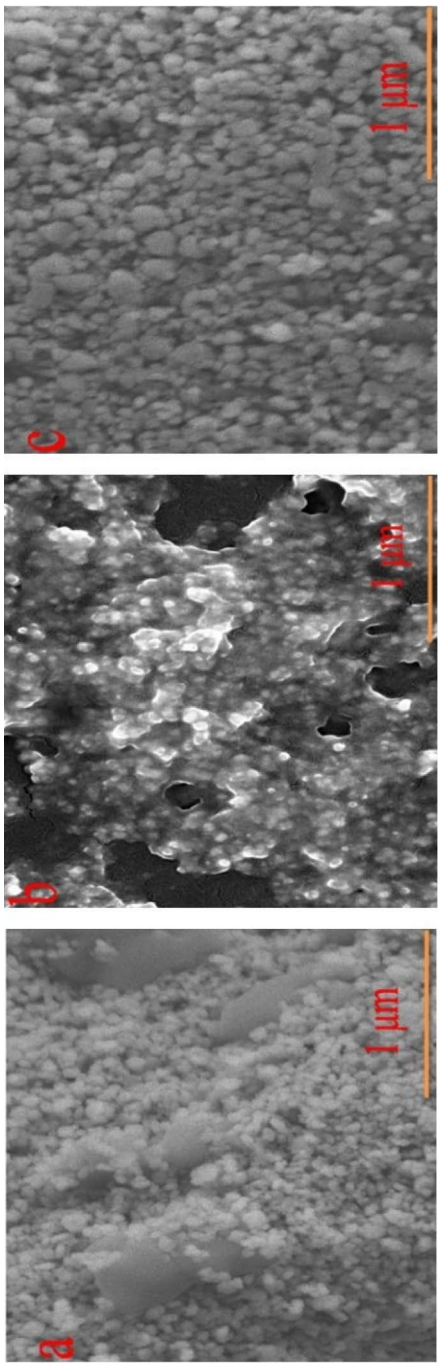

Fig. 7 FESEM images of (a) ZnO (b) Ag NPs (c) Ag doped ZnO NPs respectively

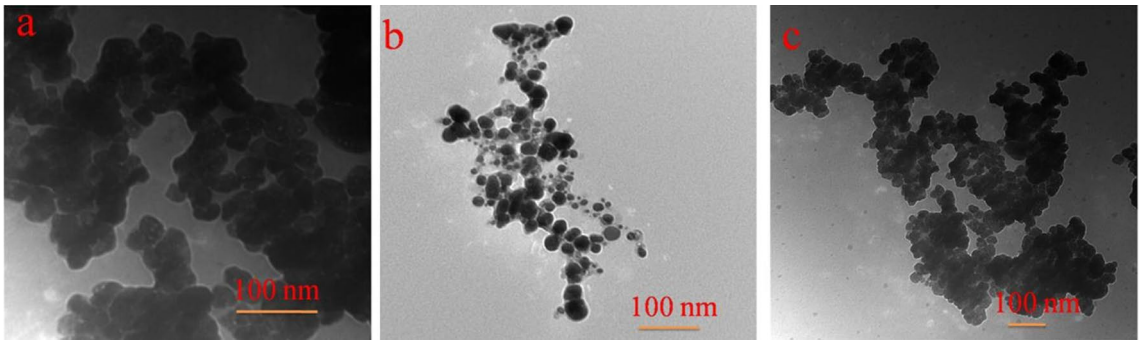

Fig. 8 TEM images of (a) ZnO (b) Ag & (c) Ag/ZnO NPs respectively

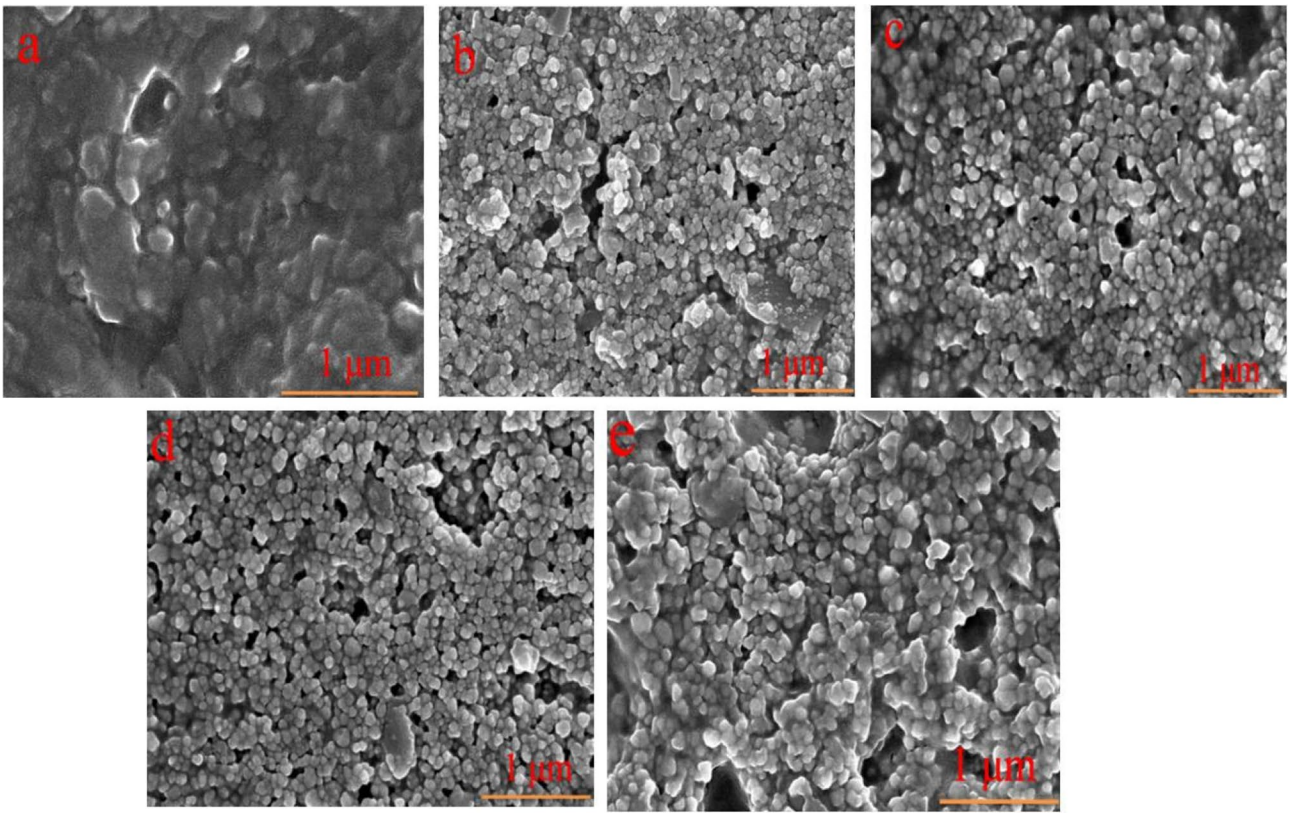

Fig. 9 FESEM images of Cur(a), Cur_Zn(b), Cur_ ZnAg(c),Cur_ZnAg1 (d),Cur_ZnAg2(e) respectively

Incorporation of ZnO and Ag/ZnO NPs in Cur has brought a drastic decrease in the content of carbon and oxygen.

As curcumin is a organic molecule having carbon, hydrogen and oxygen-based structure, ratio between carbon to oxygen has been calculated. Major decrease in C/O ratio observed (0.76 to 0.22) in Cur_Zn (Fig. 10b) as compared to pure Cur (Fig. 10a). It predicts chemical bondage between Cur and ZnO, which has been already confirmed in FTIR study (Fig. 3ii). The Cur_ZnAg2 NC (Fig. 10(e)) shows the lowest C/O ratio (0.17) may be due to maximum content of Ag/ZnO.

Furthermore, the dispersion of ZnO and Ag/ZnO in Cur matrix has been demonstrated in Fig. 11(a-i). Figure 11(a-c) depict the mapped area of carbon and oxygen element in curcumin whereas Cur_Zn confirms the mapped position of carbon, oxygen elements (Fig. 11e, f) in addition to Zinc (Fig. 11g) respectively. With the enhancement in the amount of Ag/ZnO NPs in Cur matrix in comparison to pure curcumin sample bring a drastic decrease in the mapped area of carbon (Fig. 11(i)) as compared to other elements (Fig. 11j–l) respectively. This will also predict the chemical bondage between incorporated NPs with Cur matrix.

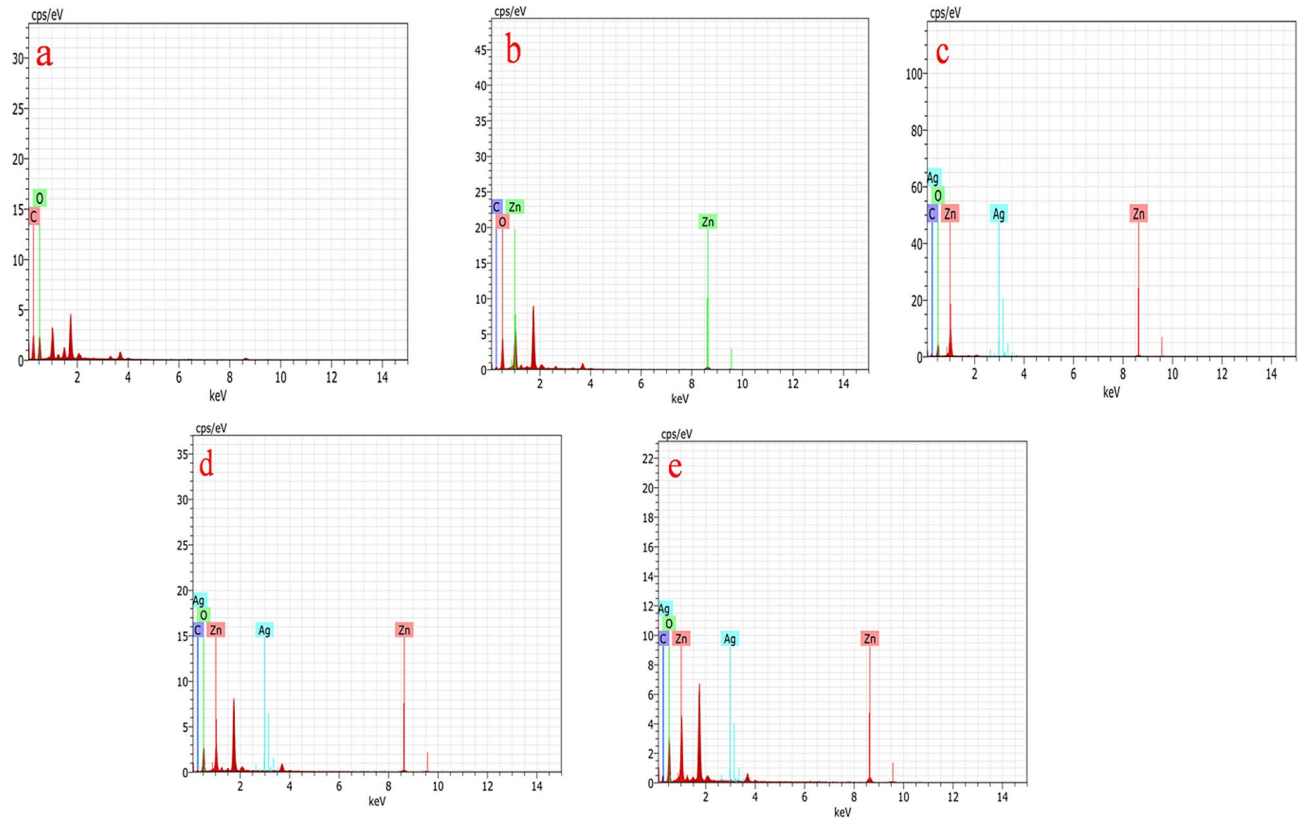

Fig. 10 EDS spectrum of Cur(a), Cur_Zn(b),Cur_ ZnAg(c),Cur_ZnAg1 (d),Cur_ZnAg2(e) respectively

The physical presence of curcumin, ZnO and Ag/ZnO in NCs has been confirmed by TEM images as shown in Fig. 12a–d. Pure curcumin shows low-density spherical entities having average diameter 137.43 nm. Average size of 40.38 nm has been observed in Cur_Zn as shown in Fig. 12b. Figure 12(b), shows ZnO NPs have a ~ 6 nm coating of Cur (~ 34.65 nm). Furthermore, the Ag/ZnO NPs in Cur (Cur_ZnAg4) (Fig. 12c), depicts higher contrast in the core of NC as compared to Cur_Zn sample, which predicts the presence of some high-density material which is silver. The width of curcumin coating on Ag/ZnO based NC has been observed ~ 5 nm as shown in Fig. 12c.

To authenticate, the core–shell theory of Ag/ZnO-Cur NCs, high resolution(HR)TEM imaging of Cur_ ZnAg2(Fig. 12 c) has been conducted in Fig. 12(d,d1,d2,d3) respectively. Figure 12d reveals the HR image of NC, which resolves the sharp crystalline behavior with the atomic d-spacing value of d = 0.242 nm of core material(ZnO)(Inset in Fig. 12(d2)). The observed d-spacing value is close to d-value (0.243 nm) of < 101 > peak observed in XRD study for Ag/ZnO NPs. In addition, the FFT image of the scanned area also shows six spots in Fig. 12d1, which further confirms the hexagonal structure of ZnO which is located in the core of NC. This will surely confirm the core–shell hypothesis of ZnO-Curcumin NCs formulation.

Furthermore, to be more precise in the statement of Cur and Ag/ZnO effective bondage, corresponding diffraction patterns have been studied in Fig. 12(d3). There is clear observation of < 101 > , < 110 > and < 201 > < hkl > plan es diffraction patterns on the basis of their corresponding d-spacing value from XRD study of Ag/ZnO (figure S1).

2.7 Water contact angle (WCA) measurement

To study the self-cleaning properties of CZNCs, the corresponding surface wettability behavior has been studied by WCA measurements and detail is demonstrated in Fig. 13. To analyze the wetting behavior of NCs surfaces, their roughness behavior also have been investigated as depicted in Fig. 14. Normally, two types of WCA behavior exist based on the attraction and repulsion between the liquid droplet and sample surface i.e. WCAs < 90° or > 90°. Depending on the WCA values, corresponding surfaces were classified as hydrophilic and hydrophobic nature [61]. Ideally, Youngs equation [62] demonstrates well-known formula for the rigid and perfectly smooth surface as shown in Eq. 4:

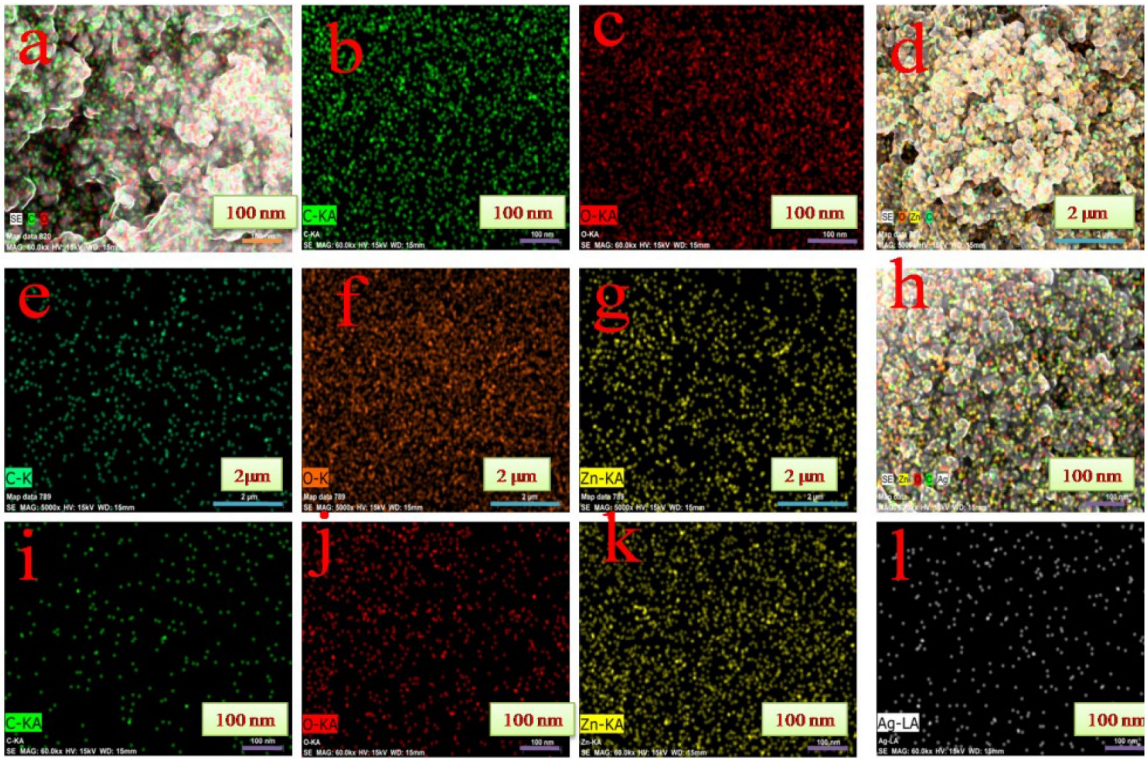

Fig. 11 FESEM mapping images of Cur sample for **a** mixed mapped area **b** mapped area of carbon **c** oxygen area; **d** mixed mapped area of Cur_Zn sample, **e** mapped area of carbon **f** oxygen area, **g** zinc mapped area; **h** mixed mapped area of Cur_ZnAg2 sample, **i** mapped area of carbon **j** oxygen area, **k** zinc mapped area, (i) silver(Ag) respectively

Table 1 Depicts the wt % of Carbon (C), Oxygen (O), Zinc(Zn), Silver(Ag), ratio of C/O for Cur, Cur_Zn, Cur_ZnAg, Cur_ZnAg1, Cur_ZnAg2 respectively

Name of sample	Carbon (wt%)	Oxygen (wt%)	Zinc (wt%)	Silver (wt%)	C/ O ratio (wt%)
Cur	43.11	56.89	–	–	0.76
Cur_Zn	5.47	25.10	27.59	–	0.22
Cur_ ZnAg	16.80	33.54	48.80	0.15	0.50
Cur_ ZnAg1	8.03	24.33	32.19	0.30	0.33
Cur_ ZnAg2	3.16	18.81	22.49	0.13	0.17

$$Cos(\theta) = \frac{(\gamma_{sv} - \gamma_{ls})}{\gamma_{lv}} \tag{4}$$

where γ_{sv}, γ_{ls}, γ_{lv} are interfacial tension between surface/vapor, liquid/solid, liquid/vapor respectively.

To demonstrate the ideal wetting behavior of any surface, the perfect flat surface must be synthesized. Surface wetting behavior of synthesized thin films can be explained via WCA measurement based on two model viz. (1) Wenzel (2) Cassie.

Basically, the roughness is the ratio of actual to projected area. In this case, the above Eq. 4, gets transformed into Eq. 5:

$$Cos\left(\theta_{rough}\right) = rCos\left(\theta_{true}\right) \tag{5}$$

In Wenzel model, higher WCA has been observed as liquid have low contact area on the rough sample surface [63] whereas in Cassie model, decrease in WCA value observed due to trapping of air packet on sample surface [64].

Entire WCA measurements on CZNCs surface have been tuned from Cur = 40.55° to 26.95°, 16.00°, 20.60°, 15.25° for Cur_Zn, Cur_ZnAg, Cur_ZnAg1, Cur_ZnAg2 respectively. Corresponding surface roughness (R_q) (nm) of studied samples get tuned from 114.20 nm to 94.38 nm, 32.74 nm, 110.90 nm, 41.01 nm (Fig. 14a–e) respectively. To expound the wetting behavior of studied thin film surfaces, the roughness will play a very crucial role. Highest WCA i.e. 40.55° (Fig. 13a) has been observed for Cur which may be due to its water repellent nature [65] with maximum roughness value (114.20 nm). Higher WCA of Cur sample can be explained as per Wenzel model explanation where buffers region at interface constructs the balancing of a water droplet with low contact area behavior. With the incorporation of ZnO

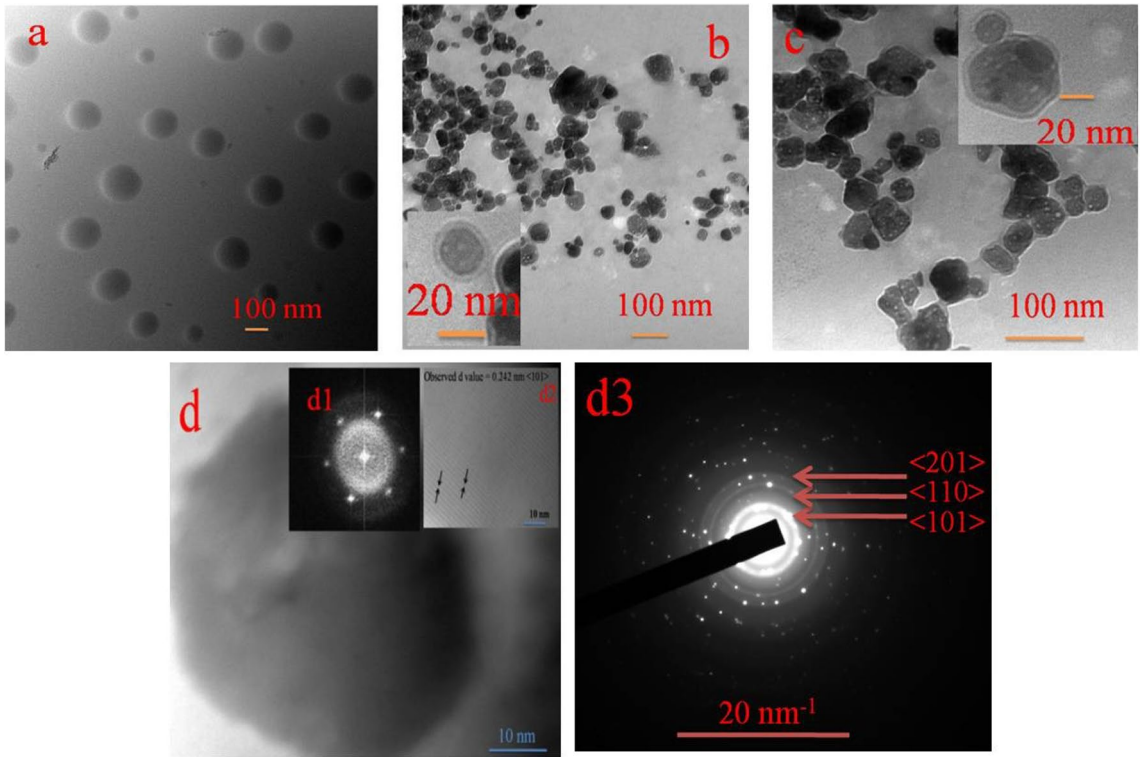

Fig. 12 TEM images of Cur(a), Cur_Zn(b),(c) Cur_ZnAg2, (d) high resolution image with its FFT representation (d1) & observed d-spacing in Cur_ZnAg2, (d3) with corresponding diffraction pattern respectively

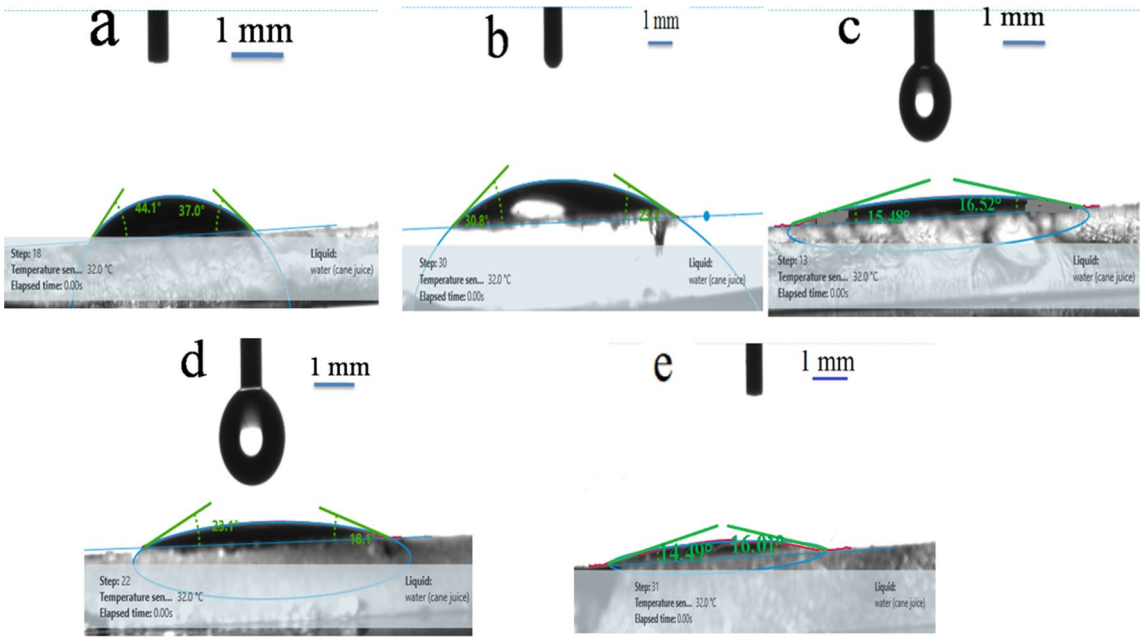

Fig. 13 WCA measurement of Cur(a), Cur_Zn(b),Cur_ ZnAg(c),Cur_ZnAg1 (d),Cur_ZnAg2(e) respectively with 10 µl of water droplet

in Cur i.e. Cur_Zn, WCA dwindle to 26.95° (Fig. 13b). The decrease in WCA can be explained for Cur_Zn sample on the basis of Cassie model with decrease in roughness to 94.38 nm. In Cur_ZnAg sample, the additional presence of Ag metal in ZnO, bring contact angle (CA) to 16.00° with a decrease in surface roughness to 32.74 nm (Fig. 13c.

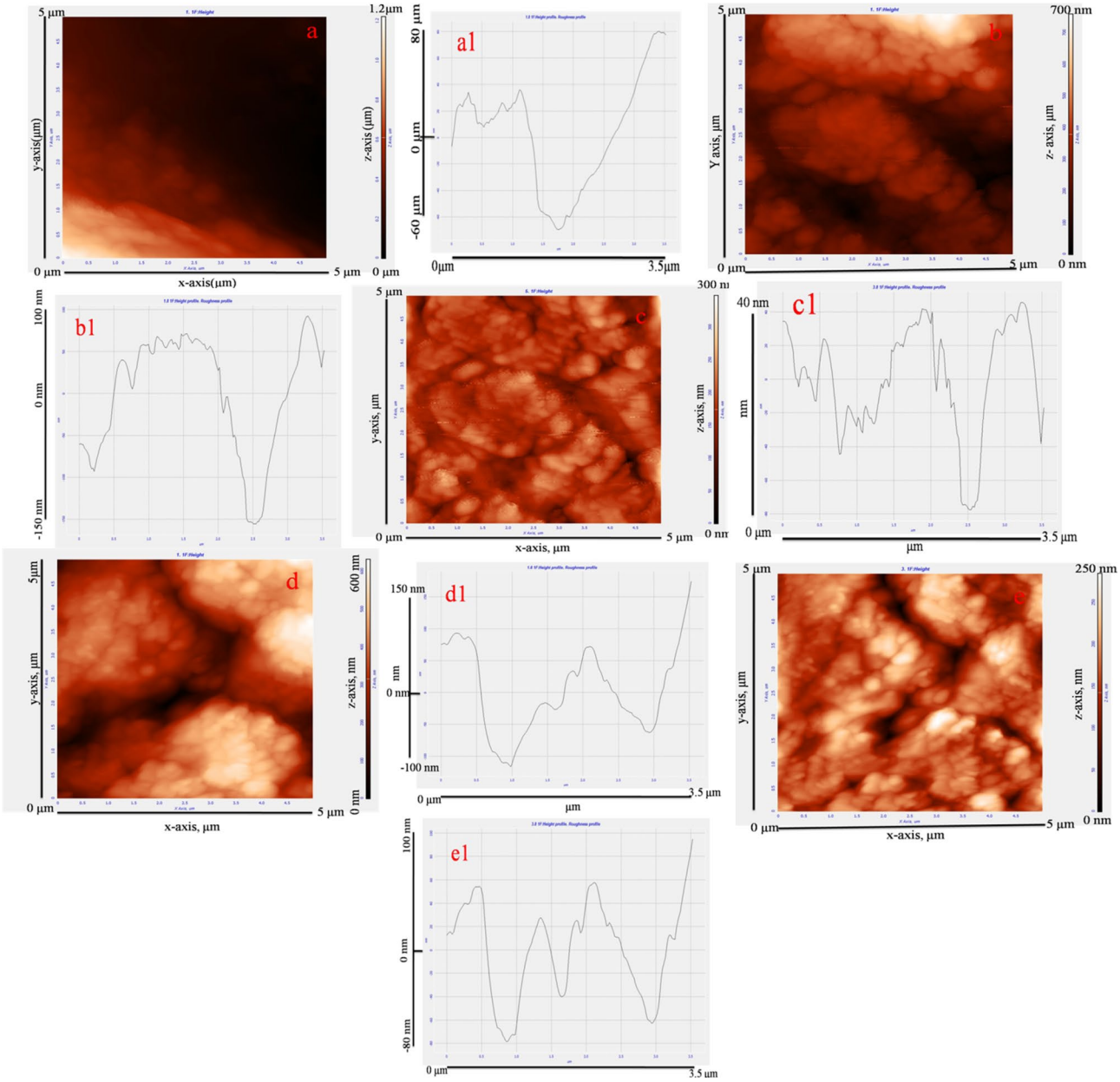

Fig. 14 AFM 2D images with their roughness profile for Cur(a & a1), Cur_Zn(b & b1), Cur_ ZnAg(c & c1), Cur_ZnAg1 (d & d1), Cur_ ZnAg2(e & e1) respectively

Moreover, in Cur_ZnAg1 sample, with a higher content of Cur as compared to Ag/ZnO NPs, CA again increases to 20.60° (Fig. 13d) with 110.90 nm roughness (as per Wenzel model) [39]. Cur_ZnAg2 sample, due to vice versa content of Cur and Ag/ZnO as compared to Cur_ZnAg1 NC, brings a decrease in CA to 15.25° (Fig. 13e). This can be explained on the basis of Cassie model. Enhanced hydrophilic nature of Cur_ZnAg2 sample may be due to the maximum content of Ag/ZnO, which brings a decrease in the oxygen packets on the sample surface with low roughness value i.e. 41.01 nm (as depicted in Fig. 10 and Table 1) [66].

Furthermore, the self-cleaning features of synthesized CZNCs can be explained with hydrophilic nature. In our case, WCA = 15.25° for Cur_ZnAg2 NC brings chemisorptions of water molecules on the sample surface as compared to Cur sample (WCA = 40.55°) have been observed. The presence of water on the sample surface adsorbs the additional water molecules through hydrogen bonding and vanderwaal forces. The adsorbed impurities on sample surface get removed by the water contact behavior through self-cleaning behavior of surface [67].

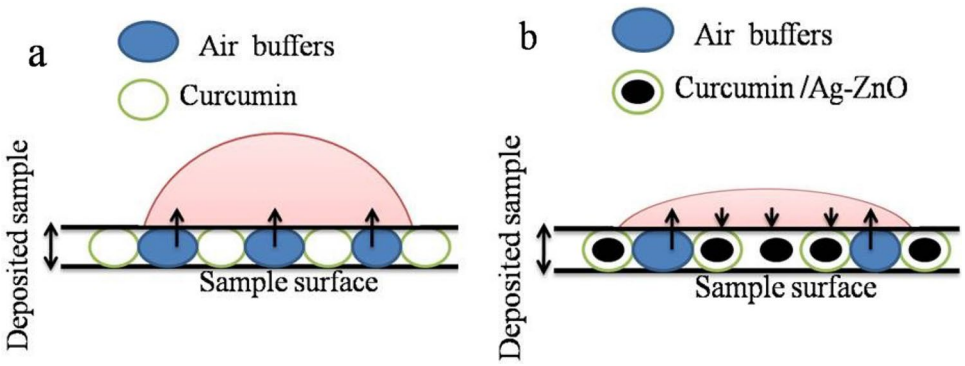

Fig. 15 Depict the water droplet behavior with **a** Cur **b** Cur-Ag/ZnO thin film respectively

2.8 Reasons for variable WCA in studied NCs towards self-cleaning mechansim

Figure 15 illustrates the schematic representation of WCA behavior with studied CZNC samples. Figure 15a, have a higher contact angle for pure curcumin(Cur) sample may be due to high roughness sites where maximum water get imbibe. This will creates buffer region between solid(sample surface)-liquid(water) interface. Observed buffer region at solid–liquid interface on sample surface will balance the water droplet. The incorporation of ZnO and Ag/ZnO NPs into Cur matrix brings the presence of air packets with a decrease in their roughness [68]. The hydroplilic behavior of CZNCs can also be explained with an increase in the amount of nanomaterial(Ag/ZnO) in Cur leads to a decrease in interfacial energy via phase inversion mechansim [43]. All these factors lead to increase in the contact area between the sample surface and water droplet which lowers the contact angle for Cur_ZnAg2 NC [40–45].

The maximum spreading of water droplet under hydroplilic behavior on CZNCs surface brought maximum interaction between droplet and sample surface. We have proposed through the current WCA behavior of CZNCs for self-cleaning process which leads towards effective removal/auto washing of deposited contaminents on the CZNCs surfaces.

3 Conclusions

A successful attempt has been made to exploit the CZNCs features of curcumin, ZnO and Ag/ZnO for self-cleaning application. Reported CZNCs tuned to core–shell formulation with optimum transmittance & lowest refractive index values i.e. 39.06%, 1.98. At 800 °C temperature, 47% weight loss has been observed for Cur_ZnAg2 as compared to pure curcumin's 82% loss, confirms the CZNCs thermal stability feature. Controlled surface roughness i.e. 41.01 nm of Cur_ZnAg2 NC bring WCA to 15.25° as compared to Cur WCA = 40.55° predicts structural level tuning of NCs. This may be due to exploitation of appropriate synthesis method, mixing components, homogenization steps, and critical evaluation of properties (structural, chemical, surface properties etc.) for surface wetting behavior. Conclusively optically active, thermally stable CZNCs having hydrophilic behavior can be utilized in self-cleaning applications.

Acknowledgements Author would like to thanks Sunpure Extract Pvt. Ltd. New Delhi (USFDA Registration No.-12953402634) for providing purified form of curcumin for research purpose. Authors also like to thanks SAIF, Panjab University for providing different characterization facilities.

Compliance with ethical standards

Conflict of interest There are no conflicts of interest to declare.

References

1. S. Gopi, J. Jacob, K. Varma, S. Jude, A. Amalraj, C.A. Arundhathy, R. George, T.R. Sreeraj, C. Divya, A.B. Kunnumakkara, Phytother. Res. **31**, 1883–1891 (2017)
2. S.C. Gupta, S. Patchva, S.B.B. Aggarwal, AAPS J **15**, 195–218 (2013)
3. A. Goel, A.B. Kunnumakkara, B.B. Aggarwal, Biochem Pharmacol. **75**, 787–809 (2009)
4. B. Aggarwal, C. Sundaram, N. Malani, H. Ichikawa, *The Molecular Targets and Therapeutic Uses of Curcumin in Health and Disease* (Springer, New York, 2007), pp. 1–75
5. K.D.K. Ahuja, D.A. Kunde, M.J. Ball, D.P. Geraghty, J Agar Food Chem **54**, 6436 (2006)
6. N.R. Jana, P. Dikshit, A. Goswami, N. Nukina, J Biol Chem. **279**, 11680 (2004)
7. G.P. Lim, T. Chu, F. Yang, W. Beech, S.A. Frautschy, G.M. Cole, J. Neurosci. **21**, 8370–8377 (2001)
8. Z.Y. Du, X. Wei, M.T. Huang, X. Zheng, Y. Liu, A.H. Conney, K. Zhang, Pharm. Res. **36**, 1204 (2013)
9. C. Chen, H. Xue, S. Mu, J. Electroanal. Chem **713**, 22 (2014)
10. C.M. Bitencourt, C.S. Favaro-Trindade, P.J.A. Sobral, R.A. Carvalho, Food Hydrocolloids **40**, 145 (2014)
11. R.C.G. Martin, H.S. Aiyer, D. Malik, Y. Li, Food Chem. Toxicol. **50**, 227 (2012)
12. B. Aggarwal, S. Shishodia, Biochem. Pharmacol. **71**, 1397 (2006)
13. A. Amalraj, A. Pius, A, S. Gopi, J. Tradit. Complem. Med. 7 (2017) 205–233

14. D. Sinha, D. De, A. Ayaz, Spectrochim. Acta A **193**, 467–474 (2018)
15. S. Prateeksha, C.V. Rao, A.K. Das, S.J.K. Barik, B.N. Singh, Mol. Pharmacut. **16**, 3399–3413 (2019)
16. Z. Sayyar, H.J. Malmiri, Crystall. Mater. **234**, 307–328 (2019)
17. K. Varaprasad, M.M. Yallapu, D. Nunez, P. Oyarzun, M. Lopez, T. Jayaramudu, C. Karthikeyan, RSC Adv. **9**, 8326 (2019)
18. R.N. Moussawi, D. Patra, Sci. Rep. **6**, 1–13 (2016)
19. Y.W. Wang, A. Cao, Y. Jiang, X. Zhang, J.H. Liu, Y. Liu, H. Wang, Appl. Mater Interfaces **6**, 2791–2798 (2014)
20. K.R. Raghupathi, R.T. Koodali, A.C. Manna, Langmuir **27**, 4020–4028 (2011)
21. S. Ghayempour, M. Montazer, M.M. Rad, Carbohydr. Polym. **139**, 232 (2016)
22. A. Kołodziejczak-Radzimska, T. Jesionowski, Materials **7**, 2833–2881 (2014)
23. Y.B. Hahn, R. Ahmad, N. Tripathy, Chem. Commun. **48**, 10369–10385 (2012)
24. Y. Jo, E. Choi, N. Choi, C.K. Kim, Ind. Eng. Chem. Res. (2016). https://doi.org/10.1021/acs.iecr.6b01510
25. A.D. Politano, K.T. Campbell, L.H. Rosenberger, R.G. Sawyer, Surg. Infect. **14**, 8–20 (2013)
26. Q. Yuan, Z.U.H. Khan, A. Ahmad, F.U. Khan, K. Tahir, M. Shakeel, S. Ullah, J. Photochem. Photobiol. B **183**, 367–373 (2018)
27. Z.U.H. Khan, A. Khan, Y. Chen, N.S. Shah, N. Muhammad, A.U. Khan, K. Tahir, F.U. Khan, B. Murtaza, S.U. Hassan, S.A. Qaisrani, P. Wan, J. Photochem. Photobiol. B **173**, 150–164 (2017)
28. T. Ghosh, A.B. Das, B. Jena, C. Pradhan, C, Front. Life Sci. **8**, 47–54 (2015)
29. A. Sandmann, A. Kompch, V. Mackert, H.L. Christian, M. Winterer, Langmuir **31**, 5701–5711 (2015)
30. A.S.H. Hameed, C. Karthikeyan, A.P. Ahamed, N. Thajuddin, N.S. Alharbi, S.A. Alharbi, G. Ravi, Sci. Rep. **6**, 24312 (2016)
31. K. Karthik, S. Dhanuskodi, C. Gobinath, S. Prabukumar, S. Sivaramakrishnan, J. Mater. Sci.: Mater. Electron **29**(2018), 5459–5471 (2018)
32. K. Karthik, S. Dhanuskodi, C. Gobinath, S. Prabukumar, S. Sivaramakrishnan, J. Phys. Chem. Solids **112**, 106–118 (2018)
33. M.R. Gholipour, T. CaoDinh, F. Béland, D. Trong-On, Nanoscale **7**, 8187–8208 (2015)
34. A.H. Zyoud, H.S. Hilal, J Phyto Chem BioSub. **8**(3), 127–137 (2014)
35. G.M. Raghavendra, T. Jayaramudu, K. Varaprasad, S. Ramesh, K.M. Raju, RSC Adv. **4**, 3494–3501 (2014)
36. P.K. Singh, V. Kotia, D. Ghosh, G.M. Mohite, A. Kumar, S.K. Maji, Chem. Neurosci. **4**, 393–407 (2013)
37. R.K. Basniwal, H.S. Buttar, V.K. Jain, N. Jain, J. Agric, Food Chem. **59**, 2056–2061 (2011)
38. B. Zheng, S. Pen, X. Zhang, D.J. McClements, J. Agric, Food chem. (2018). https://doi.org/10.1021/acs.jafc.8b03174
39. S.K. Sethi, G. Manik, Polym. Plast. Technol. Eng. (2018). https://doi.org/10.1080/03602559.2018.1447128
40. A. Syafiq, B. Vengadaesvaran, A.K. Pandey, N.A. Rahim, J. Nanomater. (2018). https://doi.org/10.1155/2018/6412601
41. R. Nosrati, A. Olad, H. Najjari, Surf. Coat. Technol. **316**, 199–209 (2017)
42. J. Hong, Y. He, Desalination **332**, 67–75 (2014)
43. B. Boopathy, A. Gangasalam, A. Mahalingam, J. Chem. Technol. Biotechnol. (2020). https://doi.org/10.1002/jctb.6462
44. P. Kumbhaskar, A. Pramanik, S. Biswas, A.K. Kole, R. Sarkar, P. Kumbhakar, J. Hazardous Mater. **360**, 193–203 (2018)
45. R. Singh, R. Sharma, P.B. Barman, D. Sharma (2017) Mater. Res. Exp. https://doi.org/10.1088/2053-1591/aa95fc
46. A. Kaur, S.K. Kansal, Nanosci. Nanotechnol. Asia **6**, 113–118 (2016)
47. F. Khan, S.-H. Baek, J.H. Kim, J Alloys Compd **682**, 232–237 (2016)
48. R.Y. Hong J.H. Li, L.L. Chen, D.Q. Liu, H.Z. Li, Y. Zheng, J. Ding, Powder Technol 189(2009) 426–432.
49. K. Elumalai, S. Velmurugan, Appl Surf Sci (2015). https://doi.org/10.1016/j.apsusc.2015.03.176
50. S. Wanninger, V. Lorenz, A. Subhan, F.T. Edelmann, Chem. Soc. Rev. **44**, 4986 (2015)
51. M.M. Yallapu, M. Jaggi, S.C. Chauhan, Colloids Surf. B **79**, 113–125 (2010)
52. D. Sinha, D. De, A. Ayaz, Spectrochim. Acta Part A Mol. Biomol. Spectrosc. **193**, 467–474 (2018)
53. S.T. Tan, B.J. Chen, X.W. Sun, X. Hu, X.H. Zhang, S.J. Chua, J Cryst Growth **281**, 571 (2005)
54. J. Tauc, Amorphous and Liquid semiconductors (1974) ISBN-978–1–4615–8705–7
55. G. Magesh, G. Bhoopathi, N. Nithya, A.P. Arun, E. Ranjith Kumar Int J Biol Macromol 117 (2018) 959–966
56. C.O. Ayieko, R.J. Musembi, S. Mwaita, B.O. Aduda, P.K. Jain, Int. J. Energy. Eng. **2**, 67–72 (2012)
57. D. Patra, R.N. Moussawi, Proceedings of the 15th IEEE International Conference on Nanotechnology July 27–30, 2015, Rome, Italy, 978–1–4673–8156–7/15.
58. S. Raj, D.R. Shankaran, Sens. Actuators B **226**, 318–325 (2016)
59. B. Sun, Y. Tian, L. Chen, Z. Jin, Food Hydrocolloids **77**, 911–920 (2018)
60. K. Varaprasad, K. Ramam, G.S. MohanReddy, R. Sadiku, RSC Adv. **4**, 60363–60370 (2014)
61. L. Wang, J. Xue, Y. Zhang, Ind. Crops Prod. **130**, 71–80 (2019)
62. G.C. Basak, L. Goswami, B. Chattopadhyay, A. Bandyopadhyay, Polym. Compos. **20**, 279–288 (2012)
63. J. Bico, C. Tordeux, D. Quéré, Colloid Surf A **206**(1–3), 41–46 (2002)
64. A.B.D. Cassie, S. Baxter, Trans. Faraday Soc. **40**, 546–551 (1944)
65. W.H. Lee, C.Y. Loo, M. Bebawy, F. Luk, R.S. Mason, R. Rohanizadeh, Curr. Neuropharmacol. **11**, 338–378 (2013)
66. C. Wang, B. Zhou, Y. Tu, M. Duan, P. Xiu, J. Li, H. Fang, Scientific Report, 2(2012) 358(1–6).
67. K. Guan, Surf Coat Tech **191**, 155–160 (2005)
68. S.A. Mahoney, T.E. Rufford, D. Johnson, A.S.K. Dmyterko, S. Rodrigues, J. Esterle, V. Rudolph, K.M. Steel, Int. J. Coal Geol. **179**, 302–315 (2017)